Effective-interaction approach to the Fermi hard-sphere system

Angela Mecca,[1,2] Alessandro Lovato,[3,4] Omar Benhar,[1,2] and Artur Polls[5]
[1]*INFN, Sezione di Roma, I-00185 Roma, Italy*
[2]*Dipartimento di Fisica, "Sapienza" University, I-00185 Roma, Italy*
[3]*Argonne Leadership Computing Facility, Argonne National Laboratory, Argonne, Illinois 60439, USA*
[4]*Physics Division, Argonne National Laboratory, Argonne, Illinois 60439, USA*
[5]*Departament d'Estructura i Constituents de la Matèria, E-08028 Barcelona, Spain*
(Received 31 October 2014; revised manuscript received 4 March 2015; published 24 March 2015)

The formalism based on correlated basis functions and the cluster-expansion technique has been recently employed to derive an effective interaction from a realistic nuclear Hamiltonian. To gauge the reliability of this scheme, we perform a systematic comparison between the results of its application to the Fermi hard-sphere system and the predictions obtained from low-density expansions, as well as from other many-body techniques. The analysis of a variety of properties, including the ground-state energy, the effective mass, and the momentum distribution, shows that the effective-interaction approach is quite accurate, thus suggesting that it may be employed to achieve a consistent description of the structure and dynamics of nuclear matter in the density region relevant to astrophysical applications.

DOI: 10.1103/PhysRevC.91.034325 PACS number(s): 24.10.Cn, 21.30.Fe

I. INTRODUCTION

Approaches based on effective interactions are widely used to study the properties of strongly interacting many-body systems, when the bare interaction between the constituents cannot be treated in perturbation theory by using the basis states describing noninteracting particles [1,2].

Effective interactions specifically designed to reproduce the bulk properties of nuclear matter (see, e.g., Refs. [3,4]), while being remarkably successful in a number of instances, fail to provide a quantitative account of nucleon-nucleon (NN) scattering, both in free space and in the nuclear medium, the understanding of which is needed for the description of nonequilibrium properties [5,6]. The results reported in Ref. [5] clearly show that the determination of the shear viscosity and thermal conductivity of pure neutron matter, relevant to many astrophysical applications [7,8], requires effective interactions derived from *ab initio* microscopic approaches capable of explaining the observed NN scattering data in the zero-density limit [5].

The authors of Refs. [9,10] have developed a procedure to determine the effective interaction in nuclear matter using the correlated basis function (CBF) formalism and the cluster-expansion technique. While this scheme has been thoroughly tested through comparison between its results and those obtained from G-matrix perturbation theory in pure neutron matter [5], the analysis of a somewhat simpler many-body system, several properties of which can be accurately calculated and expressed in analytic form, may provide further insight into the validity and robustness of the underlying assumptions.

The nucleon-nucleon (NN) interaction is known to be strongly repulsive at short distances, as clearly indicated by saturation of the charge-density distributions measured by elastic electron-nucleus scattering [11]. As a consequence, the Fermi hard-sphere fluid, i.e., a system of point-like spin $\frac{1}{2}$ particles interacting through the potential

$$v(r) = \begin{cases} \infty, & r < a \\ 0, & r > a \end{cases} \tag{1}$$

has been long recognised as a valuable model for investigating concepts and approximations employed to study the properties of nuclear matter.

In this paper we discuss the derivation of the effective interaction of the Fermi hard-sphere system within the approach of Ref. [10], as well as its application to the calculation of a variety of properties, including the energy per particle, the self-energy, the effective mass, and the momentum distribution.

As an introduction, Sec. II is devoted to a summary of the results of low-density expansions in powers of the dimensionless parameter $c = k_F a$, where a is the hard-core radius [see Eq. (1)] and k_F is the Fermi momentum. In Sec. III, we outline the basics of both CBF theory and the cluster-expansion technique, which are needed to obtain the ground-state energy and determine the effective interaction. The perturbative calculation of the self-energy at second order in the effective interaction is described in Sec. IV, while in Sec. V the single-particle properties resulting from our calculations are reported and compared to those obtained by using different approaches. Finally, in Sec. VI we summarize our findings and state the conclusions.

II. LOW-DENSITY EXPANSIONS

The expansion of the ground-state energy of the quantum-mechanical hard-sphere system in powers of the dimensionless parameter c was first discussed by Huang and Yang [12], who were able to derive its terms up to order c^2, back in the 1950s.

More recently, Bishop carried out a systematic analysis, including a comparison between results obtained by using different computational schemes [13].

The calculation of the ground-state energy exploits the formalism developed to describe a scattering process involving two particles interacting through a strongly repulsive potential. The main element of this approach is the replacement of the bare interaction with the t matrix, which amounts to including the contribution of the infinite series of ladder diagrams. This technique, which in general allows us to achieve a fast convergence of perturbative calculations, becomes essential when dealing with the hard-core interaction of Eq. (1).

The author of Ref. [13] considered two different treatments of scattering in a degenerate medium, based on the use of time-ordered Goldstone diagrams or Feynman diagrams, yielding the same expression of the ground-state energy.

For a hard-sphere system of degeneracy $\nu = 4$,[1] the result, obtained including the first four terms in the expansion, reads

$$E_0 = \frac{k_F^2}{2m}\left[\frac{3}{5} + \frac{2}{\pi}c + \frac{12}{35\pi^2}(11 - 2\ln 2)c^2 + 0.78c^3 + \frac{32}{9\pi^3}(4\pi - 3\sqrt{3})c^4 \ln c + O(c^4)\right], \tag{2}$$

where the linear term describes the effects of forward scattering, the quadratic term takes into account Pauli's exclusion principle, and the higher-order terms arise from the occurrence of processes involving at least three particles.

The low-density expansion for the single-particle spectrum, $e(k)$, and the effective mass, defined as

$$m^\star(k) = \left(\frac{1}{k}\frac{de}{dk}\right)^{-1}, \tag{3}$$

are discussed in Ref. [1]. The result at $k = k_F$, derived taking into account terms quadratic in c, is

$$\frac{m^\star(k_F)}{m} = 1 + \frac{24}{15\pi^2}(7\ln 2 - 1)c^2. \tag{4}$$

Note that the above equation implies that (i) there are no linear contributions and (ii) $[m(k_F)^\star/m] > 1$ for all values of c.

Perturbative results at order c^2 have also been obtained for the momentum distribution, defined as

$$n(k) = \langle 0|a_{\mathbf{k}}^\dagger a_{\mathbf{k}}|0\rangle, \tag{5}$$

where $|0\rangle$ denotes the system ground state, while $a_{\mathbf{k}}^\dagger$ and $a_{\mathbf{k}}$ are creation and annihilation operators, respectively [14–18]. The explicit expression of $n(k)$, obtained by the authors of Refs. [16–18] carrying out an expansion in powers of the free-space t matrix, can be found in the appendix.

III. THE CORRELATED BASIS FUNCTION EFFECTIVE INTERACTION

Within the CBF approach, the *correlated* states of the hard-sphere system are obtained from the noninteracting Fermi gas (FG) states through the transformation

$$|n\rangle = \frac{F|n_{\rm FG}\rangle}{\langle n_{\rm FG}|F^\dagger F|n_{\rm FG}\rangle^{1/2}}, \tag{6}$$

where the operator F, embodying the correlation structure induced by the interaction potential, is written in the form

$$F = \prod_{j>i} f(r_{ij}), \tag{7}$$

with

$$f(r_{ij} \leqslant a) = 0, \quad \lim_{r_{ij}\to\infty} f(r_{ij}) = 1, \tag{8}$$

where $r_{ij} = |\mathbf{r}_i - \mathbf{r}_j|$ is the interparticle distance.

In principle, the shape of the two-body correlation function, $f(r_{ij})$, at $r_{ij} > a$, can be determined from functional minimization of the expectation value of the Hamiltonian:

$$H = T + V = \sum_i \frac{k_i^2}{2m} + \sum_{j>i} v(r_{ij}), \tag{9}$$

in the correlated ground state. In the above equation, $k_i = |\mathbf{k}_i|$, m denotes the particle mass and v is the potential of Eq. (1).

The effective interaction

$$V_{\rm eff} = \sum_{j>i} v_{\rm eff}(r_{ij}), \tag{10}$$

is defined by the relation

$$\frac{1}{N}\langle H\rangle = \frac{1}{N}\frac{\langle 0|H|0\rangle}{\langle 0|0\rangle} = K_{\rm FG} + \frac{1}{N}\langle 0_{\rm FG}|V_{\rm eff}|0_{\rm FG}\rangle, \tag{11}$$

where N is the number of particles, and $K_{\rm FG} = 3k_F^2/(10m)$ is the expectation value of the kinetic energy per particle in the FG ground state. Note that the above equation implies that the CBF effective interaction is defined *not* in operator form, but in terms of its expectation value in the Fermi gas ground state.

The calculations discussed in the following sections are largely based on the assumption—that will be tested by comparing our results to those obtained from different many-body approaches—that perturbative calculations involving matrix elements of $V_{\rm eff}$ between Fermi gas states provide accurate estimates of *all* properties of the Fermi hard-sphere system.

A. Cluster-expansion formalism

The calculation of matrix elements of any many-body operator between correlated states involves largely irreducible $3N$-dimensional integrations. This problem, that becomes quickly intractable with increasing N, can be circumvented by expanding the matrix element in a series, the terms of which represent the contributions of subsystems (clusters) involving an increasing number of particles [19]. Since correlations are short ranged, at not-too-high density the cluster expansion is expected to be rapidly convergent.

The effective interaction of Ref. [10] is derived by expanding the left-hand side of Eq. (11) and keeping the two-body

[1]The hard-sphere system with $\nu = 2$ and 4 is meant to model pure neutron matter and isospin-symmetric nuclear matter, respectively. Note that in both instances the system can be described in terms of the single parameter $c = k_F a$.

cluster contribution only. The resulting expression is

$$\frac{1}{N}\langle H\rangle = \frac{3k_F^2}{10m} + (\Delta E)_2, \tag{12}$$

with

$$(\Delta E)_2 = \frac{\rho}{2}\int d^3r \frac{1}{m}\left[\nabla f(r)\right]^2\left[1-\frac{1}{\nu}\ell^2(k_F r)\right], \tag{13}$$

where ν denotes the degeneracy of the momentum eigenstates, $\rho = \nu k_F^3/(6\pi^2)$ is the particle density, and the Slater function is defined as $\ell(x) = 3(\sin x - x\cos x)/x^3$. The form of $v_{\rm eff}$ follows immediately from Eqs. (10)–(13), implying

$$v_{\rm eff}(r) = \frac{1}{m}[\nabla f(r)]^2. \tag{14}$$

As pointed out above, the shape of $f(r)$ can be obtained from the functional minimization of the Hamiltonian expectation value in the correlated ground state. Within the two-body cluster approximation, this procedure yields the Euler–Lagrange equation

$$g''(r) - g(r)\left[\frac{\Phi''(r)}{\Phi(r)} + m\lambda\right] = 0, \tag{15}$$

where

$$g(r) = f(r)\Phi(r), \tag{16}$$

with

$$\Phi(r) \equiv r\sqrt{1-\frac{1}{\nu}\ell^2(k_F r)}. \tag{17}$$

Equation (15) is solved with the boundary conditions $f(a) = 0$ and $f(d) = 1$, the additional constraint $f'(d) = 0$ being fulfilled through the introduction of the Lagrange multiplier λ. The determination of the correlation range d will be discussed in the next section.

B. Ground-state energy

The terms of the cluster expansion can be conveniently represented by diagrams, which are classified according to their topological structure. Selected classes of diagrams can be then summed up to all orders by solving a set of coupled integral equations, dubbed the Fermi hyper-netted chain (FHNC) equations [20,21].

The correlation functions obtained from the procedure outlined above and the FHNC summation scheme have been extensively used to obtain upper bounds to the ground-state energy of a variety of interacting many-body systems, including liquid helium [22], nuclear and neutron matter [23], and the Fermi hard-sphere system [24,25]. Within this approach, yielding remarkably accurate results, the correlation range d is treated as a variational parameter. Figure 1 shows the radial dependence of the correlation functions obtained from minimization of the FHNC ground-state energy at different densities, corresponding to $c = k_F a = 0.3$, 0.5, and 0.7, respectively. Note that, throughout this article, we consistently set the hard-core radius, the particle mass, and the degeneracy to the values $a = 1$ fm, $m = 1$ fm^{-1}, and $\nu = 4$.

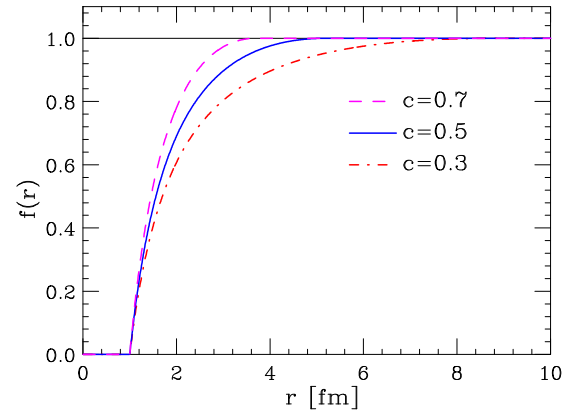

FIG. 1. (Color online) Radial dependence of the correlation functions obtained from the solution of the Euler–Lagrange equation (15). The dot-dashed, solid, and dashed lines correspond to $c = k_F a = 0.3$, 0.5, and 0.7, respectively.

The ground-state energy per particle of the Fermi hard-sphere system is usually written in the form

$$E_0 = \frac{3k_F^2}{10m}(1+\zeta), \tag{18}$$

and the low-density expansion of the parameter ζ can be readily obtained by combining its definition, Eq. (18), and Eq. (2):

$$\zeta = \frac{5}{3}\left[\frac{2}{\pi}c + \frac{12}{35\pi^2}(11-2\ln 2) + 0.78c^3 + \frac{32}{9\pi^3}(4\pi - 3\sqrt{3})c^4\ln c\right]. \tag{19}$$

In Fig. 2, the density dependence of ζ computed using Eq. (19) (dashed line) is compared to the corresponding

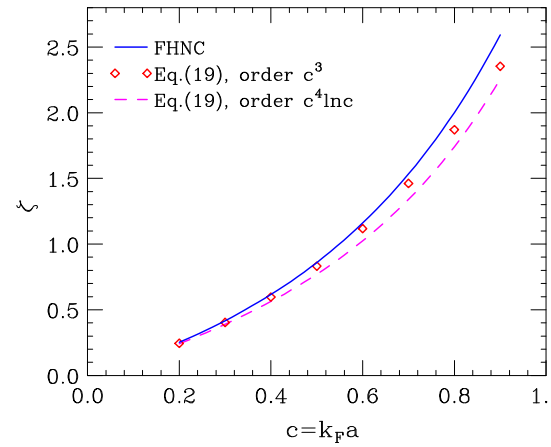

FIG. 2. (Color online) The full line shows the c dependence of the dimensionless quantity ζ, defined by Eq. (18), obtained within the FHNC approach for the system of hard spheres of radius $a = 1$ fm, mass $m = 1$ fm^{-1}, and degeneracy $\nu = 4$. The results obtained from the low-density expansion of Eq. (19) are represented by the dashed line, while the diamonds correspond to the perturbative estimates of ζ computed, neglecting terms of order higher than c^3.

FHNC result (full line). For reference, we also show, by the diamonds, the perturbative values of ζ obtained including contributions up to order c^3. It clearly appears that, at low c, corresponding to low density, the predictions of the two approaches are very close to one another. At $c = 0.2$ (0.3), the difference in ζ turns out to be less than 5% (7%), which translates into an energy difference of less than 1% (2%). The more significant discrepancies observed at higher values of c may be ascribed to a failure of the low-density expansion, although the observation that including the term of order $c^4 \log c$ leads to a decrease of ζ suggests that the contribution of cluster terms not taken into account within the FHNC scheme may also play a role. Note, however, that the full line representing the FHNC results lies consistently above the perturbative results. This pattern supports the assumption that the approximations involved in the FHNC calculation of the ground-state expectation value of the Hamiltonian do not spoil its upper-bound character.

The effective interaction, defined by Eq. (11), is designed to obtain the ground-state expectation value of the Hamiltonian at first order of perturbation theory in the Fermi gas basis. Our procedure to construct $v_{\rm eff}$ is based on the tenets that (i) FHNC calculations provide an accurate estimate of $\langle H \rangle / N$, and (ii) the FHNC results can be reproduced within the two-body cluster approximation by adjusting the correlation range d, which determines the solution of the Euler–Lagrange equation (15). From Eqs. (12)–(14), it follows that, under these assumptions, Eq. (11) is fulfilled by construction, provided its left-hand side is identified with the FHNC result.

In Fig. 3, the correlation range resulting from minimization of the FHNC ground-state energy is compared to that employed to obtain the CBF effective interaction, as a function of the dimensionless variable c. The range of the effective interaction turns out to be sizeably smaller than the correlation range obtained from the variational calculation for all values of c, the difference being ∼35% to 40%. This result is consistent with the observation that the two-body cluster approximation underestimates the FHNC energy. Therefore, reproducing the

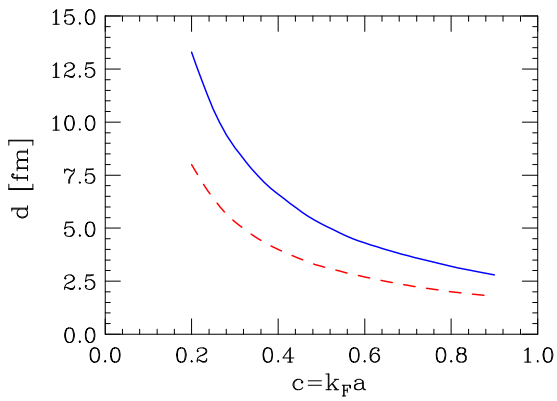

FIG. 3. (Color online) The full line shows the c dependence of the correlation range, d, resulting from minimization of the ground-state energy of the hard-sphere system computed within the FHNC approach. The dashed line corresponds to the correlation range employed to obtain the CBF effective interaction of Eq. (14).

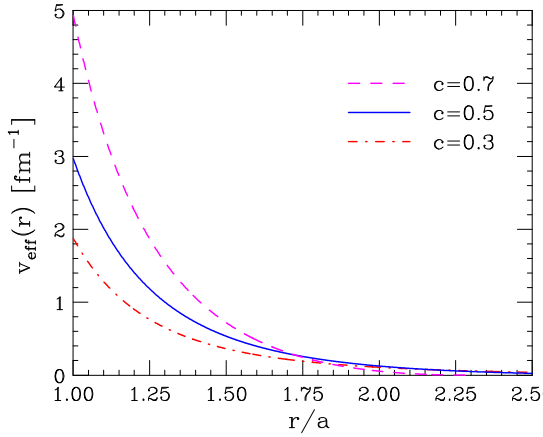

FIG. 4. (Color online) Radial dependence of the effective interaction defined by Eq. (14). The dot-dash, solid, and dashed lines correspond to $c = k_F a = 0.3$, 0.5, and 0.7, respectively. The region $(r/a) < 1$, where $v_{\rm eff}(r) = 0$, is not shown.

FHNC result at the two-body-cluster level requires a shorter correlation range, leading to a stronger effective interaction.

The radial dependence of the effective interaction defined by Eq. (14) is illustrated in Fig. 4 for three different values of the dimensionless variable c. Note that the region $(r/a) < 1$, where $v_{\rm eff}(r) = 0$, is not shown. The shape of $v_{\rm eff}$ simply reflects the fact that, as the Fermi momentum increases, the correlation range, displayed in Fig. 3, decreases, and the slope of the correlation function increases.

IV. SELF-ENERGY

The two-point Green's function G, embodying all information on single-particle properties of many-body systems, is obtained from Dyson's equation [1,26]

$$G(k,E) = G_0(k,E) + G_0(k,E)\Sigma(k,E)G(k,E), \qquad (20)$$

where G_0 is the Green's function of the noninteracting Fermi gas, the expression of which reads

$$G_0(k,E) = \frac{\theta(k-k_F)}{E - e_0(k) + i\eta} + \frac{\theta(k_F-k)}{E - e_0(k) - i\eta}. \qquad (21)$$

In the above equation, $\eta = 0^+$, $e_0(k) = k^2/(2m)$, $\theta(x)$ is the Heaviside step function, and the two terms on the right-hand side describe the propagation of particles $(k > k_F)$ and holes $(k < k_F)$.

The irreducible, or proper, self-energy $\Sigma(k,E)$ accounts for the effects of interactions. From Eqs. (20) and (21), it follows that, in interacting systems, the Green's function can be written in terms of the self-energy according to

$$G(k,E) = \frac{1}{E - e_0(k) - \Sigma(k,E)}. \qquad (22)$$

In perturbation theory, the irreducible self-energy is obtained from the expansion

$$\Sigma(k,E) = \Sigma^{(1)}(k) + \Sigma^{(2)}(k,E) + \cdots, \qquad (23)$$

where the energy-independent first-order term corresponds to the Hartree–Fock approximation, whereas the second-order

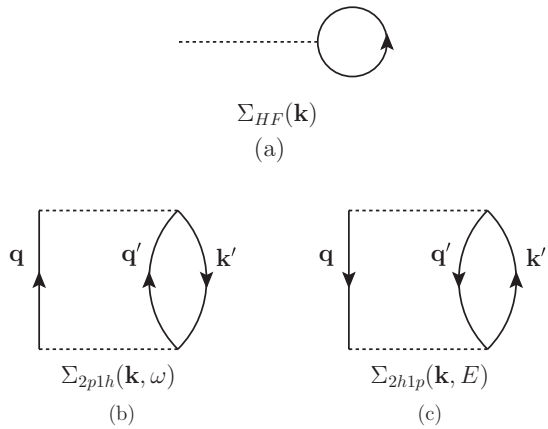

FIG. 5. Diagrammatic representation of the direct part of the first- and second-order contributions to the irreducible self-energy. Panels (a)–(c) correspond to the Hartree–Fock, polarization, and correlation terms, respectively. Dashed lines represent the CBF effective interaction, while upward- and downward-oriented solid lines depict the free propagation of particle and hole states, respectively.

terms, referred to as polarization and correlation contributions, describe interaction effects affecting the propagation of particle ($2p1h$) and hole ($2h1p$) states, respectively. The diagrams representing the direct part of the first- and second-order contribution to the irreducible self-energy are shown in Fig. 5.

The real and energy-independent Hartree–Fock contribution is obtained from

$$\Sigma_{\rm HF}(k) = \frac{1}{\nu}\sum_{\sigma,\mathbf{k}'\sigma'} n^0_<(k')\langle \mathbf{k}\sigma\mathbf{k}'\sigma'|v_{\rm eff}|\mathbf{k}\sigma\mathbf{k}'\sigma'\rangle_a, \qquad (24)$$

where $n^0_<(k) = \theta(k_F - k)$, the two-particle state is antisymmetrized according to $|\alpha\beta\rangle_a = (|\alpha\beta\rangle - |\beta\alpha\rangle)/\sqrt{2}$, and the index σ labels the discrete quantum numbers specifying the state of a particle carrying momentum $\mathbf{k}$. Equations (25) and (26) show that, because the effective interaction is diagonal

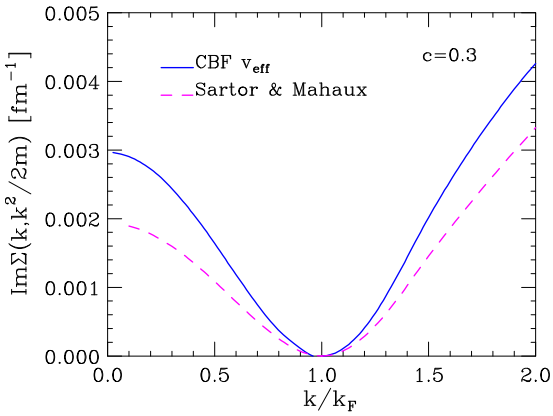

FIG. 6. (Color online) Imaginary part of the quantities $\Sigma_{2h1p}(k < k_F, k^2/(2m))$ and $\Sigma_{2p1h}(k > k_F, k^2/(2m))$, computed at $c = 0.3$ and displayed as a function of the dimensionless variable k/k_F. The solid and dashed lines correspond to the results obtained from the CBF effective interaction and from the low-density expansion of Ref. [16], respectively.

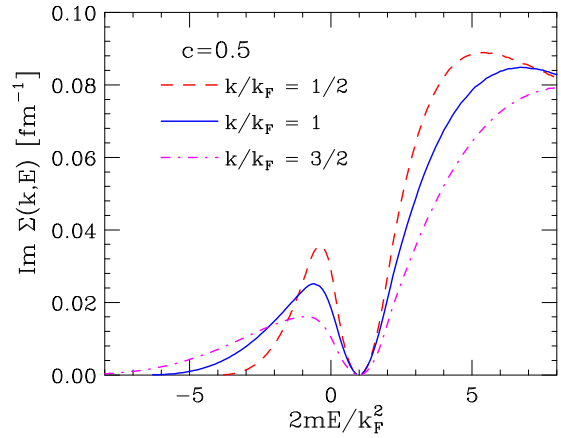

FIG. 7. (Color online) Energy dependence of the imaginary part of the polarization ($2mE/k_F^2 > 1$) and correlation ($2mE/k_F^2 < 1$) contributions to the self-energy of the Fermi hard-sphere system at $c = 0.5$. The dashed, solid, and dot-dash lines correspond to $k/k_F = 0.5$, 1, and 1.5, respectively.

in the space of the discrete quantum numbers, the self-energy does not depend on σ.

The explicit expressions of the polarization and correlation contributions are (see Fig. 5)

$$\Sigma_{2p1h}(k,E) = \frac{m}{\nu}\sum_{\sigma,\mathbf{k}'\sigma',\mathbf{q}\tau,\mathbf{q}'\tau'} \frac{|\langle \mathbf{q}\tau\mathbf{q}'\tau'|v_{\rm eff}|\mathbf{k}\sigma\mathbf{k}'\sigma'\rangle_a|^2}{q^2 + q'^2 - k'^2 - 2mE - i\eta} \times n^0_>(q)n^0_>(q')n^0_<(k'), \qquad (25)$$

and

$$\Sigma_{2h1p}(k,E) = \frac{m}{\nu}\sum_{\sigma,\mathbf{k}'\sigma',\mathbf{q}\tau,\mathbf{q}'\tau'} \frac{|\langle \mathbf{q}\tau\mathbf{q}'\tau'|v_{\rm eff}|\mathbf{k}\sigma\mathbf{k}'\sigma'\rangle_a|^2}{k'^2 - q^2 - q'^2 + 2mE - i\eta} \times n^0_<(q)n^0_<(q')n^0_>(k'), \qquad (26)$$

with $n^0_>(k) = \theta(k - k_F)$. Note that the above definitions imply that $\mathrm{Im}\Sigma_{2h1p}(k, E > k_F^2/(2m)) = \mathrm{Im}\Sigma_{2p1h}(k, E < k_F^2/(2m)) = 0$.

Figure 6 shows the behavior of the imaginary part of $\Sigma_{2h1p}(k,E)$ and $\Sigma_{2p1h}(k,E)$ corresponding to $c = 0.3$, computed at $E = k^2/(2m)$ and displayed as a function of the dimensionless variable k/k_F. For comparison, we also show the same quantities computed by Sartor and Mahaux using the low-density expansion and including terms up to order c^2 [16].

The energy dependence of the imaginary part of the second-order contributions to the self-energy is illustrated in Fig. 7, showing the results corresponding to $c = 0.5$ for three different values of momentum, corresponding to $k/k_F = 1/2$ (dashed line), 1 (solid line), and 3/2 (dot-dashed line).

V. RESULTS

The self-energy computed at second order in the CBF effective interaction, discussed in the previous section, has been used to obtain the single-particle spectrum, effective mass, and momentum distribution of the Fermi hard-sphere system.

The conceptual framework for the identification of single-particle properties in interacting many-body systems is laid down in Landau's theory of liquid ^{3}He (see, e.g., Ref. [27]), based on the tenet that there is a one-to-one correspondence between the elementary excitations of a Fermi liquid, dubbed quasiparticles, and those of the noninteracting Fermi gas.

Quasiparticle states of momentum k are specified by their energy $e(k)$ and lifetime $\tau_k = \Gamma_k^{-1}$. In the limit of small Γ_k, the Green's function describing the propagation of quasiparticles can be written in the form

$$G(k,E) = \frac{Z_k}{E - e(k) + i\Gamma_k}. \tag{27}$$

A comparison between the above expression and Eq. (22) clearly shows that quasiparticle properties can be readily related to the real and imaginary parts of the self-energy.

A. Effective mass and single-particle spectrum

The energy of a quasiparticle of momentum k, $e(k)$, is obtained by solving the equation

$$e(k) = e_0(k) + \mathrm{Re}\Sigma[k, e(k)]. \tag{28}$$

Substitution of Eq. (24) into Eq. (28) yields the Hartree–Fock spectrum, represented by the dashed lines of Fig. 8, while the results obtained including the second-order corrections to the self-energy are displayed by full lines. For comparison, the dot-dashed lines show the kinetic-energy spectrum.

From Eqs. (22) and (27) it also follows that the quasiparticle lifetime is related to the self-energy through

$$\tau_k^{-1} = \Gamma_k = Z_k \mathrm{Im}\Sigma[k, e(k)], \tag{29}$$

where

$$Z_k = \left[1 - \frac{\partial}{\partial E}\mathrm{Re}\Sigma(k,E)\right]^{-1}_{E=e(k)} \tag{30}$$

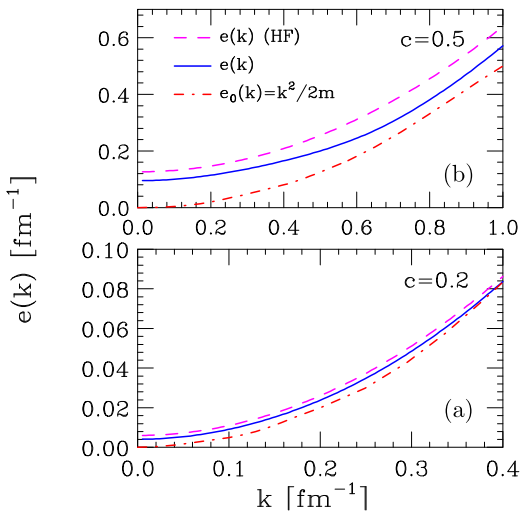

FIG. 8. (Color online) Quasiparticle energy, computed from Eq. (28) at $c = 0.2$ [panel (a)] and 0.5 [panel (b)]. The dashed and solid lines correspond to the first-order (i.e., Hartree–Fock) and second-order approximations to the self-energy, respectively. For comparison, the dot-dashed lines show the kinetic-energy spectrum.

is the residue of the Green's function of Eq. (27) at the quasiparticle pole.

Equations (28) and (29) are obtained by expanding the energy of the quasiparticle pole in powers of Γ_k and keeping the linear term only. Note that the resulting expressions of $e(k)$ and Γ_k obtained using the second-order self-energy are *not* second-order quantities.

The quasiparticle spectrum is conveniently parametrized in terms of the effective mass $m^\star$, defined by Eq. (3). The total derivative of $e = e(k)$ is performed by using Eq. (28) and keeping in mind that, since $\mathrm{Re}\Sigma(k,E)$ is evaluated at the quasiparticle pole, k and E are not independent of one another. As a consequence, one finds

$$\frac{de}{dk} = \frac{k}{m} + \frac{\partial}{\partial k}\mathrm{Re}\Sigma(k,e) + \frac{\partial}{\partial e}\mathrm{Re}\Sigma(k,e)\frac{de}{dk}, \tag{31}$$

implying

$$\frac{de}{dk} = \left[\frac{k}{m} + \frac{\partial}{\partial k}\mathrm{Re}\Sigma(k,E)\right]\left[1 - \frac{\partial}{\partial E}\mathrm{Re}\Sigma(k,E)\right]^{-1}_{E=e(k)}. \tag{32}$$

At first order the self-energy depends on k only, and the above equation reduces to

$$\frac{de}{dk} = \frac{k}{m} + \frac{\partial \Sigma_{\mathrm{HF}}(k)}{\partial k}, \tag{33}$$

with Σ_{HF} given by Eq. (24).

The dot-dash and solid lines of Fig. 9 show the c dependence of the ratio $m^\star(k_F)/m$, evaluated by using the self-energy computed at first and second order in the CBF effective interaction, respectively. It is apparent that inclusion of the energy-dependent contributions to the self-energy, resulting in a moderate correction to the spectra of Fig. 8, leads instead to a drastic change in the behavior of the effective mass. While in the Hartree–Fock approximation the ratio $m^\star(k_F)/m$ is less

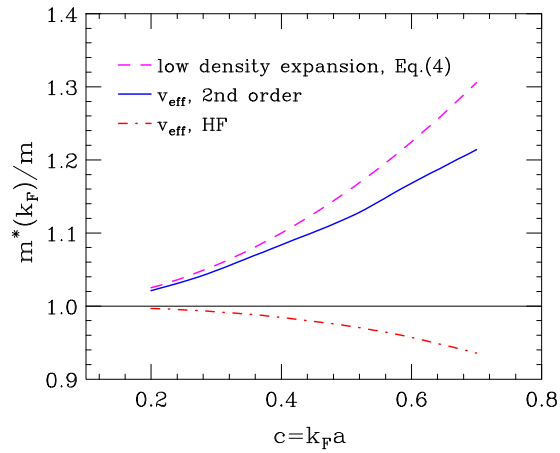

FIG. 9. (Color online) c dependence of the ratio $m^\star(k_F)/m$, obtained from Eqs. (3) and (28). The dot-dashed and solid lines represent the results of calculations carried out using the first- and second-order approximations to the self-energy. For comparison, the dashed line shows the results computed using the low-density expansion of Eq. (4).

than one and monotonically decreasing with c, the full result turns out to be larger than one and monotonically increasing.

The dashed line of Fig. 9, representing the ratio obtained from the low-density expansion at order c^2, Eq. (4), exhibits the same features as the solid line. The low-density expansion appears to provide quite accurate results for $c \lesssim 0.3$. A comparison with Fig. 2 suggests that, in the case of the ground-state energy, the inclusion of higher-order contributions extends the range of applicability of the expansion to $c \lesssim 0.4$.

It is worth pointing out that the striking differences between the effective masses computed by using the first- and second-order expressions of the self-energy are a consequence of their different functional dependencies. While the former is a function of momentum only, the latter depends on both momentum and energy. Because the enhancement of the effective mass, as well as the modification of its behavior as a function of density, arise from the appearance of the energy dependence, it is arguable that the inclusion of higher-order terms would result in small corrections.

The analysis of the momentum dependence of $e(k)$ reveals that its behavior is nearly quadratic and can be accurately parametrized in terms of $m^\star_F = m^\star(k_F)$ according to

$$e(k) = \frac{k^2}{2m^\star_F} + \text{const}, \tag{34}$$

at densities corresponding to $c \lesssim 0.5$.

B. Momentum distribution

In translationally invariant systems, the momentum distribution $n(k)$ describes the occupation probability of the single-particle state of momentum k.

The connection between $n(k)$ and the Green's function, or the self-energy, can be best understood by introducing the spectral functions appearing in the Lehmann representation of the two-point Green's function (see, e.g., Refs. [15,26]):

$$G(k,E) = \int_0^\infty dE' \left[\frac{P_p(k,E)}{E - E' - \mu + i\eta} + \frac{P_h(k,E)}{E + E' - \mu - i\eta} \right], \tag{35}$$

where $\mu = e(k_F)$ denotes the chemical potential.

The particle (hole) spectral function $P_p(k,E)$ [$P_h(k,E)$] yields the probability of adding to (removing from) the ground state a particle of momentum k, leaving the resulting $(N+1)$-particle [$(N-1)$-particle] system with energy E. It follows that

$$n(k) = \int_0^\infty dE\, P_h(k,E) = 1 - \int_0^\infty dE\, P_p(k,E). \tag{36}$$

The momentum distribution obtained from Eq. (36), with

$$P_h(k,E) = \frac{1}{\pi}\text{Im}G(k,\mu - E) = \frac{1}{\pi}\frac{\text{Im}\Sigma(k,\mu - E)}{[\mu - E - e_0(k) - \text{Re}\Sigma(k,\mu - E)]^2 + [\text{Im}\Sigma(k,\mu - E)]^2}, \tag{37}$$

and

$$P_p(k,E) = -\frac{1}{\pi}\text{Im}G(k,\mu + E) = -\frac{1}{\pi}\frac{\text{Im}\Sigma(k,\mu + E)}{[\mu + E - e_0(k) - \text{Re}\Sigma(k,\mu + E)]^2 + [\text{Im}\Sigma(k,\mu + E)]^2}, \tag{38}$$

can be cast in the form [28]

$$n(k) = Z_k \theta(k_F - k) + \delta n(k). \tag{39}$$

The first term on the right-hand side of the above equation, with Z_k defined by Eq. (30), originates from the quasiparticle pole in Eq. (27), while $\delta n(k)$ is a smooth contribution, extending to momenta both below and above k_F, arising from more complex excitations of the system. Equation (39) shows that the discontinuity of $n(k)$ at $k = k_F$ is given by

$$n(k_F - \eta) - n(k_F + \eta) = Z_{k_F} = Z. \tag{40}$$

At second order in the effective interaction, the momentum distribution obtained from Eqs. (35)–(38) can be conveniently written in the form

$$n(k) = n_<(k) + n_>(k), \tag{41}$$

where $n_<(k > k_F) = n_>(k < k_F) = 0$, and

$$n_<(k < k_F) = 1 + \left[\frac{\partial}{\partial E}\text{Re}\Sigma_{2p1h}(k,E)\right]_{E=e_0(k)}, \tag{42}$$

$$n_>(k > k_F) = -\left[\frac{\partial}{\partial E}\text{Re}\Sigma_{2h1p}(k,E)\right]_{E=e_0(k)}. \tag{43}$$

Note that the above equations imply that, within the Hartree–Fock approximation, $n(k) = \theta(k_F - k)$ and $Z = 1$.

Figure 10 shows the momentum distributions obtained including contributions up to second order in the CBF effective interaction, for three different values of the dimensionless parameter c. It clearly appears that the deviation from the Fermi gas result rapidly increases with density. A measure of interaction effects is provided by the discontinuity Z, shown in Fig. 11 as a function of c.

In Fig. 12 we compare the momentum distribution resulting from our calculation, represented by the solid line, to those reported in Ref. [24] for $c = 0.4$. The dashed line shows the results computed by using the variational wave function obtained from minimization of the ground-state energy within the FHNC scheme, while the crosses correspond to the predictions of the the low-density expansion discussed in Refs. [14,16–18] (see appendix), including contributions up to order c^2. Note that the values of $n(k > k_F)$ are multiplied by a factor of ten.

It clearly appears that the variational approach sizeably underestimates interaction effects and fails to provide the correct logarithmic behavior at k close to the Fermi momentum. On

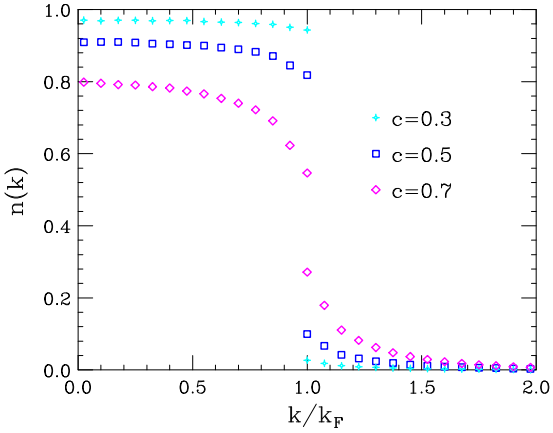

FIG. 10. (Color online) Momentum distributions computed at second order in the CBF effective interactions, for three different values of $c = k_F a$. The values of the discontinuity corresponding $c = 0.3$, 0.5, and 0.7 are 0.92, 0.72, and 0.28, respectively.

the other hand, the momentum distributions obtained from the CBF effective interaction and from the low-density expansion are in close agreement at $k < k_F$ and exhibit discontinuities that turn out to be within ∼3% of one another.

The kinetic energy computed by using the variational $n(k)$ exactly agrees with the variational energy. On the other hand, the result obtained from the perturbative momentum distribution does not necessarily reproduce the kinetic energy calculated by using the effective interaction (11), which coincides with the variational energy by definition.

In Fig. 13, the difference between the momentum distribution computed by using the effective interaction and that obtained from the low-density expansion is illustrated for different values of c, ranging from 0.2 to 0.6. The emerging picture is consistent with that observed in Figs. 2 and 9 and suggests that the low-density expansion provides accurate predictions for $c \lesssim 0.3$. Sizable discrepancies appear at larger values of c, most notably in the vicinity of the Fermi surface.

In order to establish a correspondence between the hard-sphere system and isospin-symmetric nuclear matter at equilibrium density, we analyzed the corresponding momentum

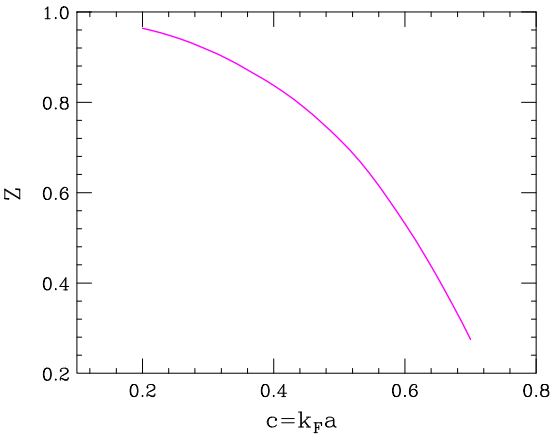

FIG. 11. (Color online) Discontinuity of the momentum distribution of the Fermi hard-sphere system, as a function of $c = k_F a$.

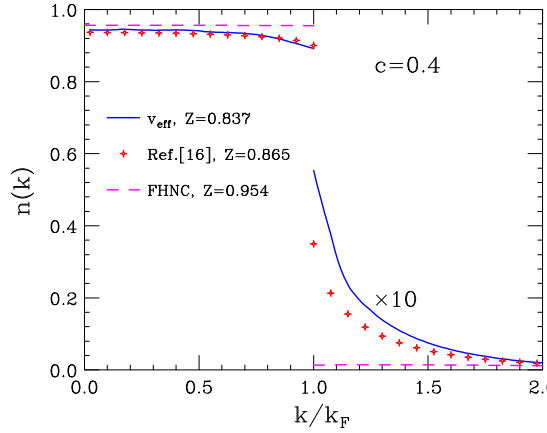

FIG. 12. (Color online) Momentum distribution of the Fermi hard-sphere system at $c = 0.4$. Solid line shows results obtained at second order in the CBF effective interaction, dashed line shows variational results of Ref. [24], crosses show results of the low-density expansion at order c^2. All values of $n(k > k_F)$ are multiplied by a factor of ten.

distributions. In Fig. 14 the results of our calculations at $c = 0.55$ are compared to the results of the the calculation of Fantoni and Pandharipande [29], carried out using a correlated wave function and including second-order contributions in CBF perturbation theory. Note that the approach of Ref. [29] is conceptually very similar to ours, although the effects of correlations are taken into account by modifying the basis states, instead of by replacing the bare potential with an effective interaction.

It appears that, as far as the momentum distribution is concerned, the system of hard spheres of radius $a = 1$ fm and $k_F = 0.55$ fm^{-1} corresponds to nuclear matter at density $\rho_{\rm NM} = 0.16$ fm^{-3}, or Fermi momentum $k_F = 1.33$ fm^{-1}.

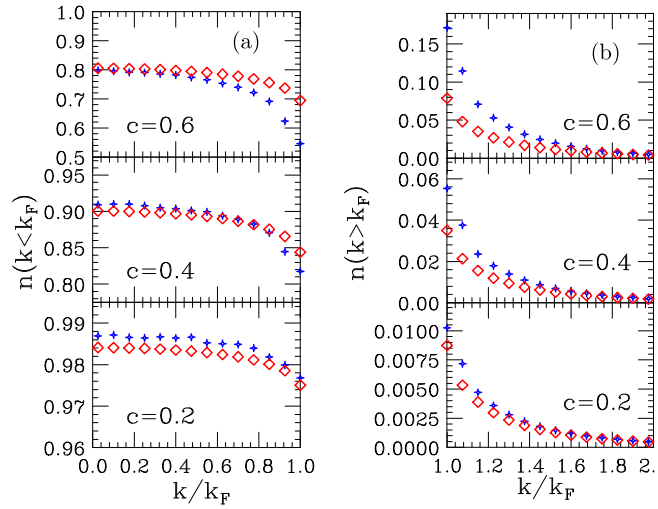

FIG. 13. (Color online) Comparison between the momentum distribution obtained from the CBF effective interactions (crosses) and the low-density expansion discussed in Refs. [14,16] (diamonds) for different values of the dimensionless parameter $c = k_F a$. Panels (a) and (b) correspond to the regions $k < k_F$ and $k > k_F$, respectively.

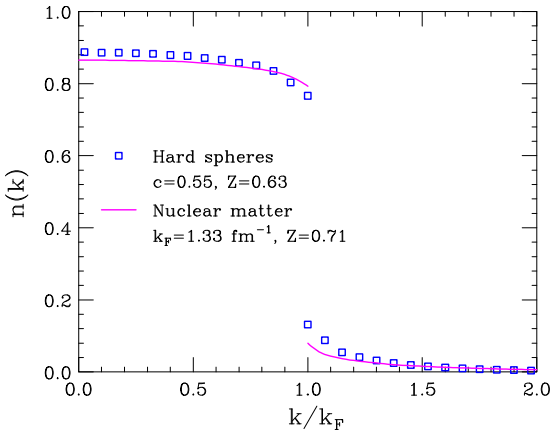

FIG. 14. (Color online) Comparison between the momentum distribution of the Fermi hard-sphere system obtained from the effective-interaction approach discussed in this article (squares) and that of isospin symmetric nuclear matter at equilibrium density reported in Ref. [29] (solid line), computed using correlated wave functions and second-order CBF perturbation theory.

Because $n(k)$ is mainly determined by the dimensionless parameter $c = k_F a$, the results of Fig. 14 suggest that nucleons in nuclear matter behave like hard spheres of radius $a = 0.55/1.33 \approx 0.4$ fm. A comparison with nuclear-matter momentum distributions obtained from other methods [30] leads to the same conclusion.

Note that, because the momentum distribution provides a measure of the occupation probability of single-particle levels, the deviations of $n(k)$ from the prediction of the Fermi gas model reflect the occurrence of virtual scattering processes involving pairs of strongly correlated particles, leading to their excitation to states outside the Fermi sea. Therefore, our results suggest that these processes are mainly driven by the short-range repulsive core of the nucleon-nucleon interaction. On the other hand, the crude description in terms of hard spheres is not expected to explain nuclear-matter properties driven by low-momentum, i.e., long-distance, physics. In this context, it is worth mentioning that the discussion of the hard-core model of nuclear matter of Ref. [1], based on the solution of the Bethe–Goldstone equation, also assumes a hard-core radius $a = 0.4$ fm.

VI. CONCLUSIONS

We carried out a perturbative calculation of the properties of the Fermi hard-sphere system by using an effective interaction derived within the CBF formalism and the cluster-expansion technique.

The proposed approach combines the effectiveness of including correlation effects through a modification of the basis states with the flexibility of perturbation theory in the Fermi gas basis. This feature is fully manifest in the calculated momentum distributions, which, unlike those obtained by using correlated wave functions in the context of the variational method, exhibit the correct logarithmic shape in the vicinity of the Fermi surface. Achieving the same result using the bare interaction and a correlated basis involves nontrivial difficulties, arising from the use of nonorthogonal perturbation theory [29].

The single-particle properties obtained from the self-energy computed using the CBF effective interaction turn out to be significantly affected by the energy-dependent second-order contributions to $\Sigma(k, E)$. In the case of the effective mass at momentum $k = k_F$, including these contributions leads to a dramatic change of both the magnitude and the density-dependence of the ratio $m^\star(k_F)/m$, with respect to the predictions of the Hartree–Fock approximation. Similar results have been found in nuclear-matter calculations, carried out within G matrix [31,32], self-consistent Green's function [33], and CBF [34] perturbation theory.

The enhancement of the effective mass has important implications for the calculation of the in-medium-scattering cross section, which in turn determines the transport coefficients, because the value of the effective mass affects both the incoming flux and the phase space available to the particles in the final state. For example, the enhanced ratio $m^\star(k_F)/m > 1$ brings about an increase of the cross section, resulting in turn in a decrease of the shear viscosity coefficient (see, e.g., Ref. [10]).

A comparison between the results discussed in this article and those obtained from low-density expansions suggests that the latter provide accurate predictions in the density range corresponding to $k_F \lesssim 0.3 - 0.4$ fm^{-1}. Note that, according to the argument of Sec. V B, these values of k_F correspond to densities in the range $0.2 \lesssim (\rho/\rho_{NM}) \lesssim 0.4$, ρ_{NM} being the equilibrium density of isospin symmetric nuclear matter.

Further insight into the accuracy of the effective-interaction approach may be gained from its extension to the study of quasiparticle scattering, which has been also investigated by using Landau's kinetic theory [35], as well as of transport properties [36].

In view of applications to dense matter of astrophysical interest, the formalism developed in this article can be readily generalized, along the line discussed in Ref. [37], to obtain a number of properties of isospin-symmetric nuclear matter at equilibrium density, such as the spectral functions defined by Eq. (35) and the density and spin-density responses [37]. Comparison between the results obtained from the CBF effective interaction and those derived from different many-body techniques and by using different nuclear Hamiltonians [37–42] will allow us to firmly assess the potential of this new approach.

ACKNOWLEDGMENTS

This research is supported by the US Department of Energy, Office of Science, Office of Nuclear Physics, under contract DE-AC02-06CH11357 (AL), MICINN (Spain), under Grant No. FI-2011-24154 and Generalitat de Catalunya, under grant 2014SGR-401 (AP), and INFN (Italy) under Grant No. MANYBODY (AM and OB). AM gratefully acknowledges the hospitality of the Departament d'Estructura i Constituents de la Matèria of the University of Barcelona, and support from "NewCompStar," COST Action MP1304.

APPENDIX: LOW-DENSITY EXPANSION OF MOMENTUM DISTRIBUTION

For the sake of completeness, we report the explicit expression of the momentum distribution obtained from the low-density expansion including terms of order up to $c^2 = (k_F a)^2$. As pointed out in Sec. V B, $n(k)$ can be conveniently written in terms of two contributions, associated with hole and particle states, according to

$$n(k) = n_<(k) + n_>(k), \tag{A1}$$

where

$$n_<(k) = 0 \text{ for } k > k_F, \quad n_>(k) = 0 \text{ for } k < k_F. \tag{A2}$$

At $x = k/k_F < 1$, the algebraic expression of $n_<(k)$, derived by the authors of Refs. [16,18], reads

$$n_<(k) = 1 - \frac{\nu - 1}{3\pi^2 x} c^2 \left[(7\ln 2 - 8)x^3 + (10 - 3\ln 2)x + 2\ln\frac{1+x}{1-x} - 2(2-x^2)^{3/2} \ln\frac{(2-x^2)^{1/2} + x}{(2-x)^{1/2} - x} \right], \tag{A3}$$

where ν denotes the degeneracy of the momentum eigenstates. The form of $n_>(k)$, reported in Refs. [16,17], depends on the range of x. For $1 < x < \sqrt{2}$,

$$n_>(k) = \frac{\nu - 1}{6\pi^2 x} c^2 \left\{ (7x^3 - 3x - 6)\ln\frac{x-1}{x+1} + (7x^3 - 3x + 2)\ln 2 - 8x^3 + 22x^2 + 6x - 24 \right.$$
$$\left. + 2(2-x^2)^{3/2} \left[\ln\frac{2 + x + (2-x^2)^{1/2}}{2 + x - (2-x^2)^{1/2}} + \ln\frac{1 + (2-x^2)^{1/2}}{1 - (2-x^2)^{1/2}} - 2\ln\frac{x + (2-x^2)^{1/2}}{x - (2-x^2)^{1/2}} \right] \right\}, \tag{A4}$$

while for $\sqrt{2} < x < 3$,

$$n_>(k) = \frac{\nu - 1}{6\pi^2 x} c^2 \left\{ (7x^3 - 3x - 6)\ln\frac{x-1}{x+1} + (7x^3 - 3x + 2)\ln 2 - 8x^3 + 22x^2 + 6x - 24 \right.$$
$$\left. - 4(x^2-2)^{3/2} \left[\tan^{-1}\frac{(x+2)}{(x^2-2)^{1/2}} + \tan^{-1}(x^2-2)^{-1/2} - 2\tan^{-1} x(x^2-2)^{-1/2} \right] \right\}. \tag{A5}$$

Finally, in the domain $x > 3$,

$$n_>(k) = 2\frac{\nu - 1}{3\pi^2 x} c^2 \left\{ 2\ln\frac{x+1}{x-1} - 2x + (x^2-2)^{3/2} \right.$$
$$\left. \times \left[2\tan^{-1} x(x^2-2)^{-1/2} - \tan^{-1}(x-2)(x^2-2)^{-1/2} - \tan^{-1}(x+2)(x^2-2)^{-1/2} \right] \right\}. \tag{A6}$$

[1] A. L. Fetter and J. D. Walecka, *Quantum Theory of Many-Particle Systems* (McGraw-Hill, New York, 1971).
[2] P. Ring and P. Schuck, *The Nuclear Many-Body Problem* (Springer, Berlin-Heidelberg, 1998).
[3] J. R. Stone, J. C. Miller, R. Koncewicz, P. D. Stevenson, and M. R. Strayer, Phys. Rev. C **68**, 034324 (2003).
[4] E. Chabanat, P. Bonche, P. Haensel, J. Meyer, and R. Schaeffer, Nucl. Phys. A **627**, 710 (1997).
[5] O. Benhar, A. Polls, M. Valli, and I. Vidaña, Phys. Rev. C **81**, 024305 (2010).
[6] H. F. Zhang, U. Lombardo, and W. Zuo, Phys. Rev. C **82**, 015805 (2010).
[7] N. Andersson, G. L. Comer, and K. Glampedakis, Nucl. Phys. A **763**, 212 (2005).
[8] G. Shen and S. Reddy, Phys. Rev. C **89**, 032802(R) (2014).
[9] S. Cowell and V. R. Pandharipande, Phys. Rev. C **73**, 025801 (2006).
[10] O. Benhar and M. Valli, Phys. Rev. Lett. **99**, 232501 (2007).
[11] B. Frois and C. N. Papanicolas, Annu. Rev. Nucl. Sci. **37**, 133 (1987).
[12] K. Huang and C. N. Yang, Phys. Rev. **105**, 767 (1957).
[13] R. F. Bishop, Ann. Phys. (NY) **77**, 106 (1973).
[14] V. M. Galitskii, Sov. Phys. JETP **7**, 104 (1958).
[15] W. Czyz and K. Gottfried, Nucl. Phys. **21**, 676 (1960).
[16] R. Sartor and C. Mahaux, Phys. Rev. C **21**, 1546 (1980).
[17] R. Sartor and C. Mahaux, Phys. Rev. C **25**, 677 (1982).
[18] V. A. Belyakov, JETP **13**, 850 (1961).
[19] J. W. Clark, Prog. Part. Nucl. Phys. **2**, 89 (1979).
[20] S. Fantoni and S. Rosati, Nuovo Cimento A **20**, 179 (1974).
[21] S. Fantoni and S. Rosati, Nuovo Cimento A **25**, 593 (1975).
[22] A. Fabrocini, S. Fantoni, and S. Moroni, Phys. Lett. B **58**, 11607 (1998).
[23] A. Lovato, O. Benhar, S. Fantoni, and K. E. Schmidt, Phys. Rev. C **85**, 024003 (2012).
[24] A. Fabrocini, S. Fantoni, A. Polls, and S. Rosati, Nuovo Cimento A **56**, 33 (1980).
[25] F. Arias de Saavedra, F. Mazzanti, J. Boronat, and A. Polls, Phys. Rev. A **85**, 033615 (2012).
[26] W. H. Dickhoff and D. Van Neck, *Many-Body Theory Exposed!* (World Scientific, Singapore, 2008).

[27] A. A. Abrikosov, L. P. Gorkov, and I. E. Dzyaloshinski, *Methods of Quantum Field Theory in Statistical Physics* (Dover, New York, 1975).
[28] O. Benhar, A. Fabrocini, and S. Fantoni, Phys. Rev. C **41**, R24 (1990).
[29] S. Fantoni and V. R. Pandharipande, Nucl. Phys. A **427**, 473 (1984).
[30] A. Rios, A. Polls, and W. H. Dickhoff, Phys. Rev. C **79**, 064308 (2009).
[31] J. P. Jeukenne, A. Lejeune, and C. Mahaux, Phys. Rep. **25**, 83 (1976).
[32] W. Zuo, I. Bombaci, and U. Lombardo, Phys. Rev. C **60**, 024605 (1999).
[33] A. Rios, A. Polls, and I. Vidaña, Phys. Rev. C **79**, 025802 (2009).
[34] S. Fantoni, B. L. Friman, and V. R. Pandharipande, Nucl. Phys. A **399**, 51 (1983).
[35] F. Mohling and J. C. Rainwater, J. Low Temp. Phys. **20**, 243 (1975).
[36] J. C. Rainwater and F. Mohling, J. Low Temp. Phys. **23**, 519 (1976).
[37] A. Lovato, C. Losa, and O. Benhar, Nucl. Phys. A **901**, 22 (2013).
[38] A. Ramos, A. Polls, and W. H. Dickhoff, Nucl. Phys. A **503**, 1 (1989).
[39] O. Benhar, A. Fabrocini, and S. Fantoni, Nucl. Phys. A **505**, 267 (1989).
[40] O. Benhar, A. Fabrocini, and S. Fantoni, Nucl. Phys. A **550**, 201 (1992).
[41] M. Baldo, A. Polls, A. Rios, H.-J. Schulze, and I. Vidaña, Phys. Rev. C **86**, 064001 (2012).
[42] A. Carbone, A. Polls, and A. Rios, Phys. Rev. C **88**, 044302 (2013).